ASME Journal of Turbomachinery
Online journal at:
https://asmedigitalcollection.asme.org/turbomachinery

Large Eddy Simulation Investigation of Film Cooling in Rotating Detonation Combustors

S. Ramanagar-Sridhara[1]
Department of Industrial Engineering,
University of Florence,
Via S. Marta 3,
Florence 50139, Italy

Antonio Andreini
Department of Industrial Engineering,
University of Florence,
Via S. Marta 3,
Florence 50139, Italy

Marc D. Polanka
Air Force Institute of Technology,
Wright-Patterson Air Force Base,
Dayton, OH 45433

Myles D. Bohon
Chair of Pressure Gain Combustion
Technische Universität Berlin,
Berlin 10623, Germany

High-power density combustors like rotating detonation combustors (RDC) offer significant benefits. However, they must overcome many challenges to be integrated into a gas turbine. Cooling the RDC is one of the most significant, due to the high heat loads generated by the combustion process. Preliminary analysis of the required cooling system has shown that cold-side convective cooling is insufficient to cool combustor walls unless a protective barrier is applied to the hot-side surface. Therefore, this work explores the feasibility of film cooling an RDC. A high-fidelity large eddy simulation investigation was employed due to the uniqueness of this problem. Namely, it was expected that the detonation wave and the downstream oblique shock wave would have a significant impact on the flow exiting cooling holes for this type of combustor. This investigation represents the first attempt to integrate a full coverage film cooling scheme in an RDC. The reference RDC geometry is provided by TU Berlin. Three different coolant plenum pressures were simulated generating three different coolant mass flows in the post-detonation region. The results showed there is a period when each hole is effectively "blocked," and coolant does not flow out of the hole. As the detonation wave passes, the film is able to recover and reform along the outer wall of the RDC. This process occurs at the detonation frequency of 7.5 kHz creating an unsteady, periodic flow behavior. Overall, the average gas temperature near the wall shows a significant reduction with the use of film cooling. These early results suggest that film cooling can be applied in an RDC flow field.
[DOI: 10.1115/1.4068987]

Keywords: rotating detonation combustor, detonation combustion, heat transfer and film cooling

1 Introduction

The Rotating Detonation Combustor (RDC) is one of the most advantageous implementations of PGC because of lower unsteadiness and easier integration with no moving parts [1]. There are several configurations of rotating detonation combustors, with different shapes [2] and sizes [3–5]. One of the most used configurations is an annular RDC where the combustion process happens in a narrow annulus with fuel and air supplied from the head end and the burnt products are expanded out of the aft end. The detonation wave continuously loops around this circular annulus. A sufficiently high mass flowrate of detonatable mixture is required to sustain the detonation wave due to its high consumption speed. The flow field of an annular RDC is shown in Fig. 1.

The structure of the flow field is characterized by a detonation front with a trailing oblique shock. This oblique shock extends to the outlet and travels with the same speed in the laboratory frame of reference as the detonation, however the shock strength and relative Mach number are significantly lower. The bulk flow exiting the combustor is mainly axial with minimal tangential component. This configuration presents essentially two distinct regions in the combustion chamber with respect to consideration of the cooling requirements. One is characterized by the passage of the detonation front, while the other, further downstream, is characterized by the burnt gas expansion and the passage of the oblique shock wave.

Thermal management and optimization of cooling systems for gas turbine (GT) engines are important because they have an impact on overall efficiency. RDCs, due to a small annulus width, highly compressible and highly unsteady flow, and high temperature gases close to the walls, generate peak heat transfer levels at least an order of magnitude greater than the conventional GT combustors. However, the global average heat transfer values fall in a range which is still manageable by the cooling systems.

Several previous research efforts have dealt with the evaluation of the thermal load in RDCs, both experimentally and numerically. Early investigations on the topic have been performed by Theuerkauf et al. [7–10]. This series of investigations considered a water-cooled RDC and, by means of experiments and numerical simulations, investigated both instantaneous and average heat fluxes. The results indicated heat flux peaks of 25 MW/m^2. However, averaged results indicated smaller values and showed an almost constant average heat flux along the axial direction of

Paper presented at the Turbo Expo, June 24–28, 2024.
[1]Corresponding author.
Contributed by International Gas Turbine Institute (IGTI) of ASME for publication in the JOURNAL OF TURBOMACHINERY. Manuscript received July 29, 2024; final manuscript received June 10, 2025; published online July 21, 2025. Tech. Editor: David G. Bogard.

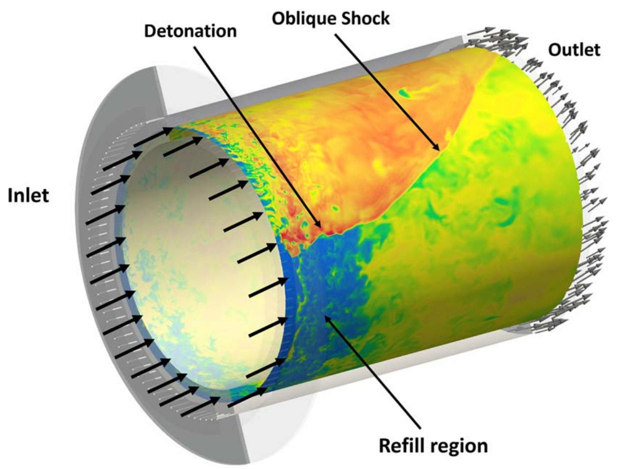

Fig. 1 Schematic of the rotating detonation combustor obtained from Ref. [6]

the RDC close to $1\,MW/m^2$. Meanwhile, numerical results have indicated an increasing and then decreasing profile of the average heat flux along the walls of the RDC, with a maximum value of $2.5\,MW/m^2$. Meyer et al. [11,12] showed that the heat flux increases with increasing wave speed, independently of the mass flow considered. The results of Meyer et al. have indicated a bulk heat flux well below $0.5\,MW/m^2$. However, higher heat flux values up to $5\,MW/m^2$ have been measured by Goto et al. [13].

Considering all the available thermal loads from the literature, Sandri et al. [14] performed a preliminary cooling requirement analysis. The outcome of their analysis showed that the combustion air alone as a coolant is no longer sufficient to optimally cool the RDC with convective cold-side cooling strategies due to its thermal capacitance. They suggested that air can be used as a barrier to protect and cool the walls, and when provided as a film can protect the walls from the hot gases and even if it is disrupted by the shock wave it can rebuild itself. Hence, film cooling can be a possible solution to reduce the thermal load on the RDC walls.

Some researchers have studied film cooling in a RDC. Tian et al. [15] were the first ones to perform computational fluid dynamics (CFD) calculations of a premixed film cooled RDC. Their geometry consisted of six film cooling holes arranged as a single-column spanning from the inlet to the outlet. Using premixed hydrogen air fed by virtual micro nozzles, they performed a complete three-dimensional unsteady Reynolds-averaged Navier–Stokes (URANS) combustion computation using ANSYS FLUENT. The outcome of their study was that the film cooling holes placed in the detonation region experienced hot gas ingestion to the coolant plenum. However, the duration of the ingestion was small when compared to the entire wave cycle. The film cooling holes placed in the oblique shock region experienced minimal ingestion, and the coolant flow was always active throughout the cycle. The film cooling had a minimal impact on the detonation cycle and the observed frequency was similar in the cooled and uncooled cases. Furthermore, the time-averaged temperature profiles show a benefit in using film cooling.

Yu et al. [16] performed similar CFD analyses with one column of film cooling holes and varying coolant mass flows. They looked at RDC thrust performance and film effectiveness with varying the mass flow. The obtained results claim that the cooling flow deforms the detonation wave but it soon recovers to its actual profile and the cooling does not quench the detonation. The increase in the coolant mass flow helps in a better film formation and increased cooling effectiveness. Li et al. [17] performed a numerical investigation on a rocket-based detonation engine with film cooling. Their geometry consists of an RDC with diverging nozzle and eight film cooling holes arranged as a single column. The numerical investigations were performed using ANSYS FLUENT by solving unsteady reactive RANS equation with *k*–*w* SST turbulence models. They worked with different hole shapes with varying coolant velocities.

All the investigations conducted by different research groups were performed with a small RDC in a premixed configuration. Furthermore, their cooling schemes include just one or two columns of film cooling holes, and the investigations were performed by solving URANS equations. To assess the consequences of film cooling in an RDC, it is necessary to conduct a thorough investigation of non-premixed RDC that is entirely cooled with film cooling. Large eddy simulations (LESs) provide a more accurate prediction of gas mixing than URANS simulations by solving for most of the turbulent length scales. URANS with the isotropic turbulence models fails to capture the significant fluidic structures that promote mixing. In the RDC, sustenance and propagation of the detonation wave are more sensitive to the reactive mixture quality. LES is needed to precisely predict the mixing in the refill region and the mixing of the coolant gases to assess the overall implications. In this context, large eddy simulations are performed for the TU Berlin RDC with the outer wall cooled by film cooling. The average gas temperature profiles near the wall along with the variation in coolant mass flow and the hot gas ingestion response are discussed in detail.

2 Film Cooling Configuration

The non-premixed TU Berlin RDC architecture [18–20] shown in Fig. 2(*a*) was implemented with film cooling to perform high-fidelity simulations. The pressure contour for the same rig without film cooling obtained by Nassini et al. [20] is depicted in Fig. 2(*a*). The region below 0.04 m is termed as the detonation region because of the presence of the high-pressure detonation wave. The region above 0.04 m is called the oblique shock region. In the current film cooling design, the film holes are distributed only in the oblique shock region, highlighted by the red dotted lines in Fig. 2(*a*), at locations from 0.04 m to 0.08 m. The detonation region was excluded from film cooling to reduce the possibility of detonation quenching due to reactant dilution caused by coolant

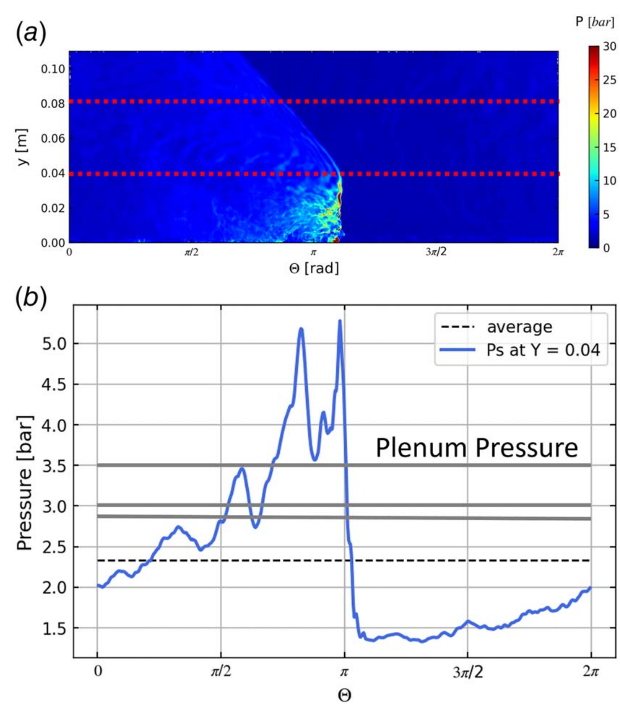

Fig. 2 (*a*) Pressure contour of the uncooled TU Berlin RDC. The region within the two dotted lines represents the film cooled region, and (*b*) circumferential variation of the static pressure at an axial position of 0.04 m along with the chosen plenum pressure.

mixing. Moreover, Tian et al. [15] observed hot gas ingestion into the coolant plenum in the detonation region.

The highlighted region was populated with typical film cooling holes with a diameter (Φ) of 1 mm and an inclination of 30 deg along with a wall thickness of 3 mm corresponding to an *L/D* ratio of 6. A classical staggered arrangement with pitch of 5.8 Φ in *X*- and 4.7 Φ in the *Y*-direction was applied. By implementing this distribution scheme, the combustor was covered with a total of 480 holes. These holes were fed from a common coolant plenum. The coolant plenum pressure (Pcool) was chosen based on the circumferential distribution of static pressure at the axial position of 0.04 m where the first row of film cooling holes is situated. The circumferential variation of the static pressure is plotted in Fig. 2(*b*). Due to the oblique shock, the peak pressure reaches a maximum of 5.5 bar, and the lowest pressure is ahead of the oblique shock which corresponds to 1.4 bar. The average pressure of the cycle was calculated to be 2.4 bar. To ensure a positive coolant supply, the plenum pressure should always be greater than the average pressure. To assess the hot gas ingestion to the coolant plenum and to know the response of recovery from hole blockage due to oblique shock, three plenum pressures of 3.5, 3.0, and 2.75 bar were chosen. This achieved coolant mass flows of 40, 68, and 112 g/s in the simulations.

3 Numerical Model

In this investigation, large eddy simulations are performed using the AVBP code developed by CERFACS. AVBP solves fully compressible, multi-species, reactive Navier–Stokes equations [21]. It uses different solving schemes like Taylor–Galerkin TTG4A (fourth-order in time and third order in space) and Lax Wendroff (second-order in space and time). AVBP is extensively validated for all kinds of flows including film cooling [21–24]. The current numerical methodology, grid sizing, and the solver setup is based on the validated uncooled RDC setup used by Nassini et al. [20]. Nassini et al. used the TU Berlin RDC setup without film cooling to study the mixing characteristics in the refill region. These previous results were validated by comparing their computations against experimental measurements taken at TU Berlin. These measurements included the plenum pressures, mass flowrates, time-resolved and averaged pressures within the combustion chamber, the total pressure at the exit of the combustor, and the pressure gain. This same RDC injector configuration was modified by adding film cooling holes in the current investigation. While no experimental measurements with film cooled outer walls are currently available, the previous validation in the uncooled configuration and similarity of major features of the cooled configurations indicate that at least the qualitative effects should be replicated, if not also the quantitative.

The explicit time integration is carried out enforcing a dynamically maximum Courant–Friedrichs–Lewy (CFL) of 0.7 resulting in a time-step of 6×10^{-9} s. The WALE LES model along with the localized artificial diffusivity model is used to stabilize the solving scheme. The hydrogen air detonation is modeled using 4S1R single-step reaction scheme developed by Nassini et al. [20]. The current reaction mechanism is compatible with the Lax Wendroff convection scheme. The single-step reaction mechanism uses four species H_2, O_2, H_2O, and N_2 in a single reaction. The solver setup along with the time-step convergence and the reaction mechanisms used for the simulation were validated by Nassini et al. [20].

The computational domain includes the TU Berlin RDC test rig along with the injectors, plenums, and film cooling holes as shown in Fig. 3(*a*). The combustor is designed with an annulus width of 7.6 mm and an outer wall diameter is 90 mm. The combustor operates with hydrogen and air.The TU Berlin RDC test rig includes 100 fuel injectors with a diameter of 0.5 mm and a circumferentially constant air gap of 1 mm for air supply inside combustion chamber. The test rig was fully discretized with pure tetrahedral mesh with an overall

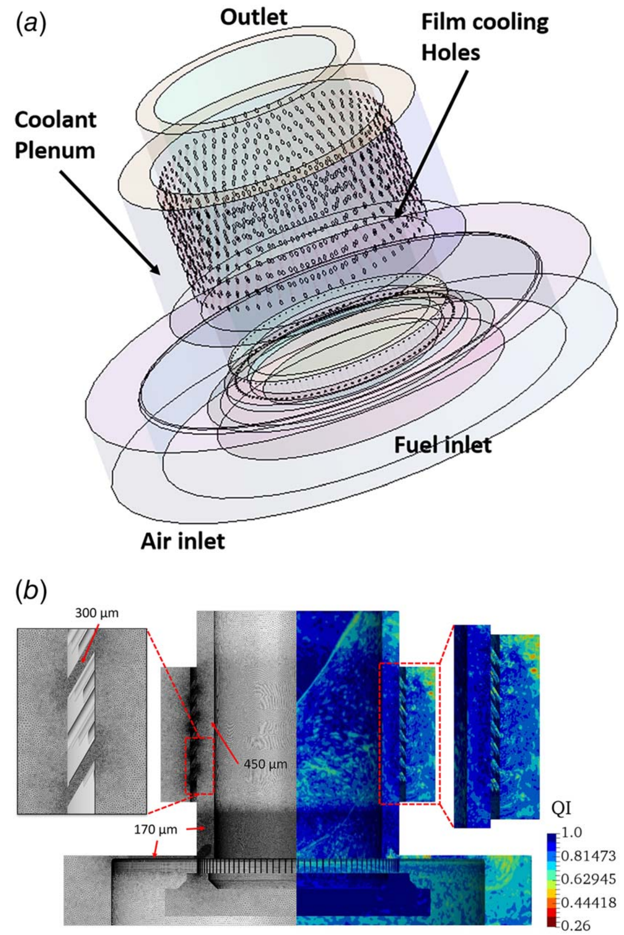

Fig. 3 (*a*) Film cooled TU Berlin RDC geometry and (*b*) section of mesh grid used for simulation and the obtained quality index after the combustion simulation. Image obtained from Ramanagar et al. [25].

mesh count of 380 million elements. The fuel injectors were discretized with a spacing of 80 μm along with 170 μm for the air gap, and the refill region which covers 20 mm starting from the injectors. The coolant holes were discretized with a spacing of 300 μm and their surrounding regions with 450 μm as shown inFig. 3(*b*).

The mesh includes a total of 380 million tetrahedron cells. This size of a mesh demands high resources. The calculations were performed on a high performance computing (HPC) cluster at the University of Florence. The cluster nodes count two 32 core AMD processors clocking 2.5 GHz. Due to the mesh size and small time-step, each simulation required 200,000 CPU hours. Non-reflecting Navier–Stokes characteristics (NSCBC) are used for inlets specifying pressure and temperature to obtain the desired mass flow. The outlet pressure of 101,325 Pa is set with the NSCBC pressure outlet boundary condition.

This study deals with the preliminary assessment of film cooling in an RDC. As a first step, heat transfer to the walls was neglected in the current study. Hence, the walls were modeled with turbulent adiabatic wall functions available on AVBP which gives an advantage of not using prism layers to capture the boundary layer. Due to the adiabatic wall assumption, wall temperatures cannot be computed, which leads to an overestimation of coolant performance and an underestimation of thermal load because of the unrealistic development of the thermal boundary layer. Nevertheless, for preliminary high-fidelity studies, this assumption allows for valuable insights into be drawn by analyzing gas temperatures outside the boundary layers. The average y^+ in the film cooling region varied between 30 and 40 while in the detonation region they were in the range of

20-80. The maximum and minimum y^+ in the detonation region correspond to 2 and 150 near the detonation respectively. A range between 30 and 300 is said to be a valid functioning range of wall models. Due to the absence of prism layer and the isotropic mesh generation, the values of x^+ and z^+ were similar to y^+. The wall functions implemented in AVBP and its sensitivity analysis for film cooling cases along with its validation was performed by Dupuy et al. and others in the literature [21,26]. Similar strategies have been applied for film cooling LES. Aillaud et al. [27] have performed film cooling simulations of a DLR turbine test rig using AVBP by specifying adiabatic no slip walls. Shum-Kivan et al. [28] performed LES of a round impinging jet using AVBP by specifying adiabatic no-slip walls for non heat transfer simulations. Agarwal et al. [29] performed LES of a single-film cooling hole using AVBP by specifying adiabatic no-slip wall. Since the current study is not calculating heat transfer measurements, adiabatic walls are sufficient for this analysis.

To initiate the detonation, the hot combustor flow field is interpolated from the previous simulation without film cooling. The obtained Celik's quality index for the current grid is shown in the right image of Fig. 3(*b*). The Celik's quality index is calculated using Eq. (1), where QI_v is the quality index, μ_{sg} is the sub grid viscosity, and μ is the molecular viscosity [30]. The quality index in the refill region was found to vary between 0.7 and 0.9, while in the film cooling region it was found to be between 0.9 and 1.0. For a good LES simulation quality index of 0.8 and above is expected. The obtained quality index and the y^+ values for current calculations are within acceptable ranges, which is indicative of a good large eddy simulation.

$$QI_v = \frac{1}{1 + 0.05(\mu_{sg}/\mu)^{0.53}} \tag{1}$$

Table 1 Summary of the simulated cases, imposed coolant plenum pressures along with the achieved coolant mass flows and chamber pressure

Pcool (bar)	$\dot{m}_{air}$ g/s	$\dot{m}_{fuel}$ g/s	$\dot{m}_{coolant}$ g/s	Mass ratio %	Pchamber (bar)	Detonation height cm	Pcool / Pchamber
No film	430	13.2	0	0	1.3	4.5	0
2.75	430	13.2	40	9.3	1.55	4	1.77
3	430	13.2	68	15.8	1.7	3.5	1.76
3.5	430	13.2	112	26	2	3	1.75

4 Results

The baseline flow condition was taken from Nassini et al. [20] and consists of an air flowrate of 430 g/s and a fuel flowrate of 13.2 g/s creating an overall chamber equivalence ratio of 1.0. The overall chamber mass flux corresponds to 290 kg/m^2 s. The detonation height for the baseline case was nominally 4.5 cm. The film cooling holes were placed downstream of the detonation in the region of the oblique shock. Three plenum pressures of 2.75, 3.0, and 3.5 bar were established to provide film cooling to this downstream region. The total mass flow achieved by imposing the three plenum pressures are reported in Table 1. The mass flow was computed at the inlet boundary patch specified for the coolant plenum. The three plenum pressures resulted in mass flows corresponding to 9%, 16%, and 26% of the core mass flow. These levels represent a realistic range of cooling flowrates as they fall below the levels found in typical gas turbine combustors where 30–40% is used for cooling the liners [31,32].

The addition of film cooling air forms an aerodynamic restriction to the combusted products and hence increases the chamber pressure. This is quite similar to how an RDC with outlet restrictions mimics the increase in the back pressure. Film cooling in the RDC behaves in a similar way by providing a flow restriction due to small annulus width and increasing the back pressure. For a case without film cooling, the obtained chamber pressure is 1.3 bar. For a film cooled RDC operating with the same inlet fuel and air mass flow as the uncooled case, the addition of 40 g/s of coolant mass flow, which corresponds to 9.3% of combustor total inlet mass flow, increases the chamber pressure to 1.55 bar. Similarly, for 15.8% mass ratio, the pressure increases to 1.7 bar, and for 26% the obtained chamber pressure is 2 bar. The increase in the chamber pressure impacts the detonation by reducing the detonation height. The height of the detonation measured by looking at the heat release profiles is reported in Table 1.

The impact on the detonation is visible in the temperature contour depicted in Fig. 4. These contours are obtained from the previous studies of Ramanagar et al. [25]. The contours represent the gas

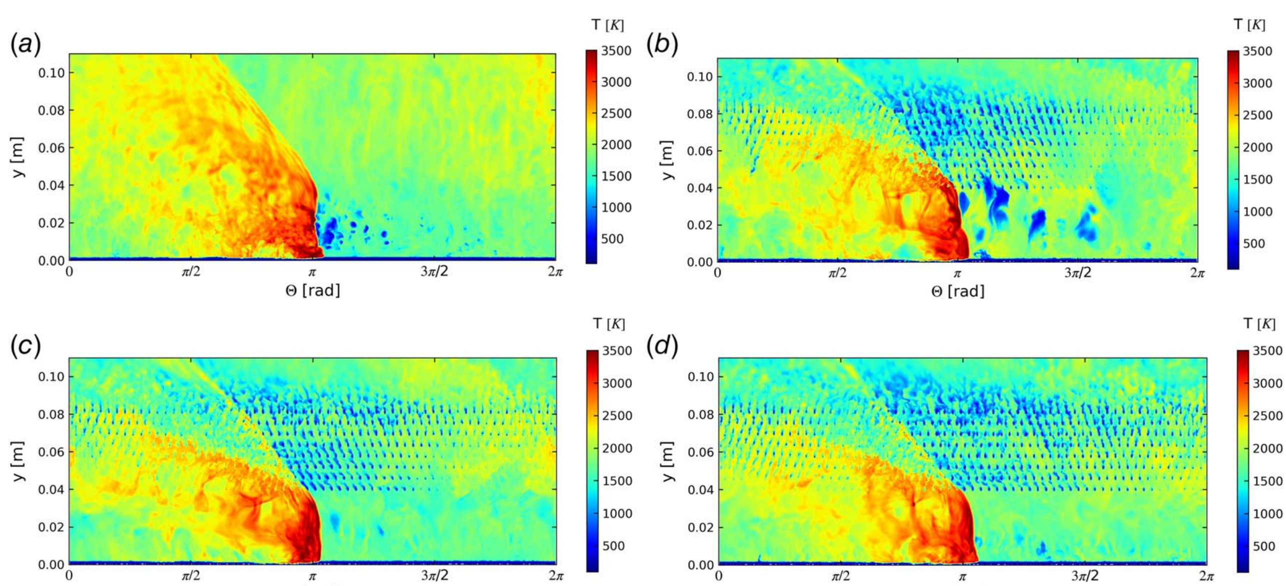

Fig. 4 Temperature of the outer wall revealing the impact of the detonation on the film cooling for three cooling pressure levels: (*a*) no film, (*b*) Pcool = 2.75 bar, (*c*) Pcool = 3.0 bar, and (*d*) Pcool = 3.5 bar. Obtained from Ramanagar et al. [25].

temperature obtained on the outer wall for the adiabatic wall solution.The temperature values presented in the current and subsequent sections should not be interpreted as material or wall temperatures for realistic applications due to the adiabatic wall assumption. For the case without film cooling, the detonation wave is nearly vertical with a height of 4.5 cm. As film cooling is added at 2.75 bar, the shape of the detonation remains mostly vertical while the height decreases to 4 cm. Further increases in cooling pressure to 3 and 3.5 bar creates a backward leaning detonation wave with a height of 3.5 and 3.0 cm, respectively. The increase in the chamber pressure due to the coolant addition impacts the detonation quality. As the film cooling flowrate increased from "no film" to 3.5 bar, the peak pressure found in the chamber increased from 19 bar to 21 bar (at 2.75 bar) to 22 bar (at 3 bar), and to 25 bar at (3.5 bar). The corresponding wave speeds were 1950 m/s, 1960 m/s, 1985 m/s, and 2070 m/s, respectively.

For the film cooled cases, the reduction in temperature is clearly visible starting from the axial height of 0.04 m. Also apparent is that the oblique shock disrupts the film leaving the film holes, thereby reducing the coolant supply as indicated by the disappearance of the holes in the region behind the detonation wave/oblique shock. After the oblique shock passes, the film eventually recovers and continues to cool the wall. Behind the oblique shock (and especially in the regions less then $\pi/2$) an increase in temperature in the film cooled region can be observed. This is attributed to deflagrative burning of the coolant caused by the reaction of unburnt hydrogen with the oxygen in the coolant. These secondary reactions are clearly visible in the contour of heat release obtained on the outer wall shown in Fig. 5. As in the temperature contours of Fig. 4, the detonation is located at the position π. The peak heat release was always found to be in the detonation wave region and is always in the range of $3.4 - 4.4 \times 10^{12}$ W/m^3. In contrast, the deflagration heat release is four orders of magnitude lower with values between 3×10^9 W/m^3 and 5×10^9 W/m^3. Therefore, the heat release contours shown are scaled to the values found for deflagration to highlight the impact of the secondary combustion.

For the uncooled case, aft of 4.0 cm, the deflagration primarily only occurred along and just downstream of the oblique shock. Low heat release levels were present in front of the oblique shock. The oblique shock causes a line of deflagrative heat release, possibly due to the increase in pressure and temperature behind the shock, which enhances the reactivity of the mixture. However, for the film cooled RDC, another region of secondary heat release was observed behind the oblique shock. This was located slightly downstream of the oblique shock after a period of lower heat release. This region of low heat release was consistent with the period of the cycle when the film cooling flow was blocked off by the shock wave (discussed in the next subsection). As the film starts to recover, a high level of heat release occurs surrounding each cooling hole. Clearly as the coolant is ejected from the holes, it mixes with the hydrogen present in the freestream flow and burns locally. This local combustion aligns with the slip line region in the RDC flow field, but more significantly, with the extremely rich buffer region resulting from the disparity in injector recovery times between the fuel and air injectors. Nassini et al. showed that for these cases, the faster recovery of the hydrogen jets results in a highly rich band. From the current results, it appears that the injection of fresh cooling air results in a significant portion of secondary heat release through deflagration as this buffer hydrogen burns. This effect is also similar to the secondary burning phenomena shown by Polanka et al. [33,34] in a non-detonating environment.

As the coolant plenum pressure was increased to 3.0 bar, the region of coolant burning increased, and heat release due to deflagration is greater. The highest deflagration heat release above 4.0 cm is observed with the coolant plenum pressure of 3.5 bar due to the high availability of oxygen for secondary reaction. For all the coolant flows, the coolant deflagration in the region trailing the shock from nominally 0 to $\pi/2$ happens closer to the wall. As the coolant flow reestablishes, a full layer of coolant protects the near wall region and lower heat release on the outer wall is experienced as seen in the region from π to 2π. Any deflagration burning that is occurring in this region happens further away from the wall due to the higher penetration of coolant into the hot gas stream (not shown).

4.1 Characterization of Coolant Ingestion.

The impact of the coolant plenum pressure on the film cooling behavior in the TU Berlin RDC was studied at three different phase angles with respect to the shock location. These three time instances were established relative to the shock being aligned at π, as shown by the location of a cut plane (the black dotted line) on the left hand image of temperature contours shown in Fig. 6. The image on the right represents the temperature contour obtained on the cut plane during those time frames. At each of these three time instances, the

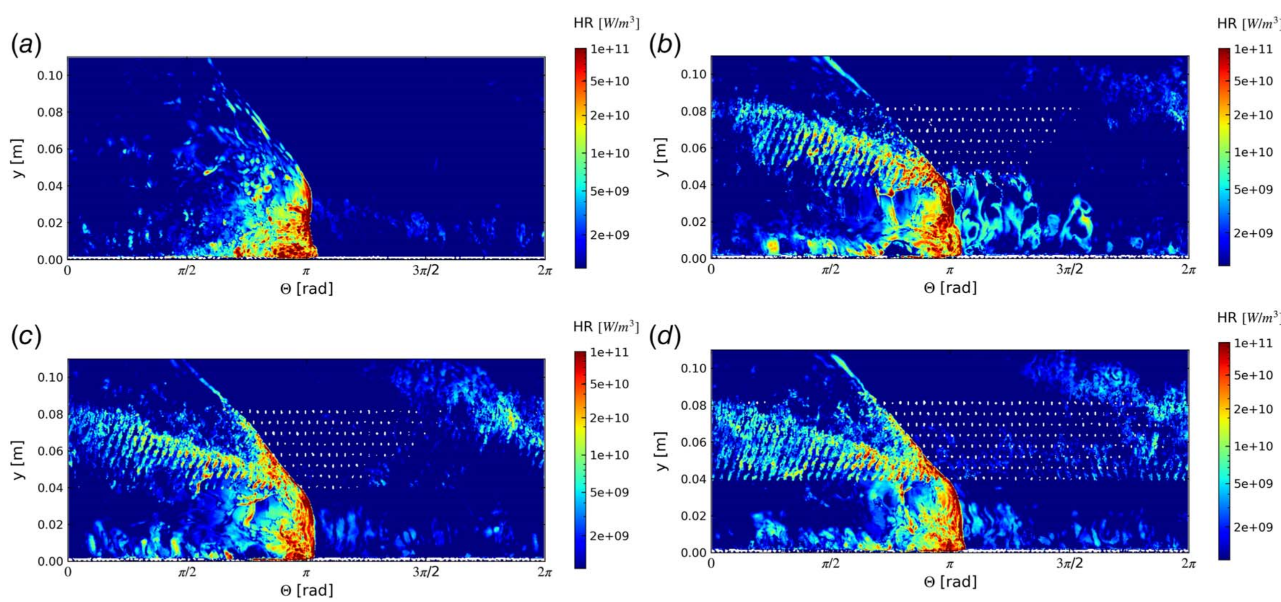

Fig. 5 Contour of heat release obtained on the outer wall for all the cases: (*a*) no film, (*b*) Pcool = 2.75 bar, (*c*) Pcool = 3.0 bar, and (*d*) Pcool = 3.5 bar

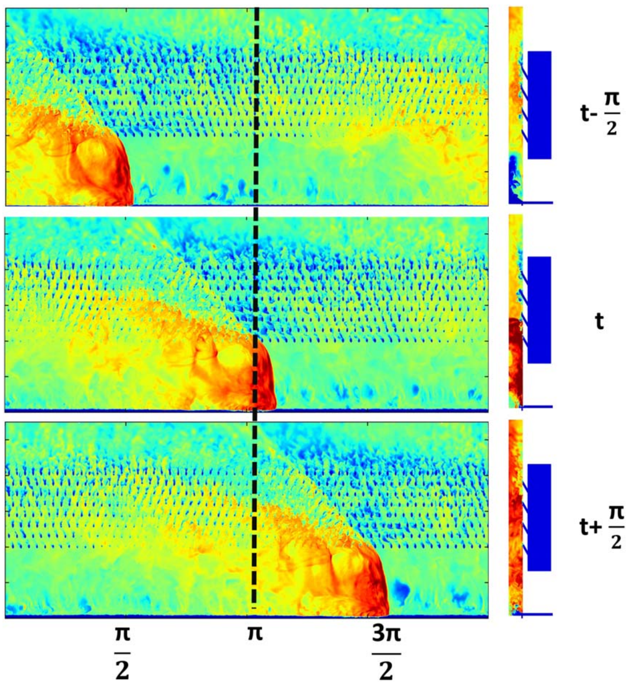

Fig. 6 Temperature contours obtained for Pcool = 3.5 bar along with the representation of the cut plane and time instances used for analysis

impact of the oblique shock on the film cooling performance was investigated for each plenum pressure. t represents when the detonation is at π, while $t+\pi/2$ is a condition when expanded gases from the detonation are passing the cut plane, and $t-\pi/2$ represents a time when the detonation has not reached the cut plane.

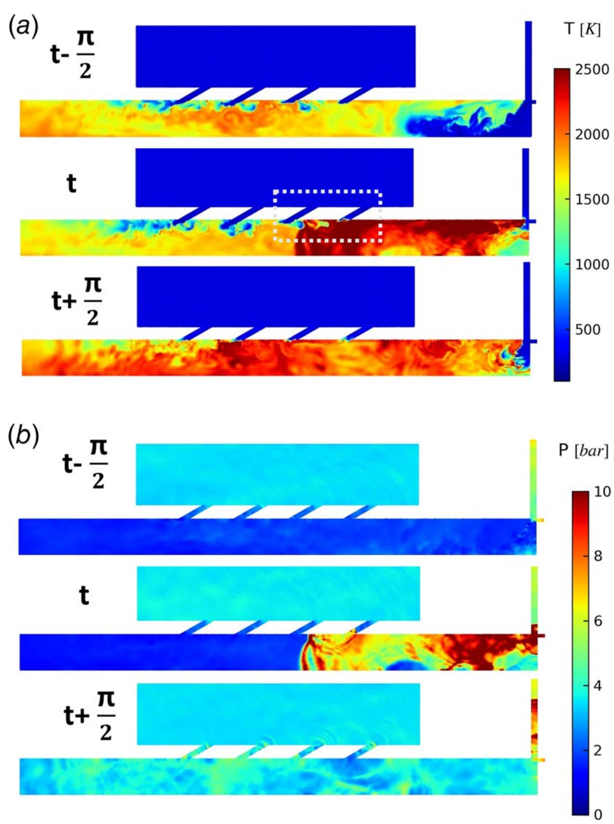

Fig. 7 (*a*) Temperature and (*b*) static pressure contour obtained at $t-\pi/2$, t, and $t+\pi/2$ for a coolant plenum pressure of 3.5 bar

The temperature and pressure contours obtained through the cut plane at $t-\pi/2$, t, and $t+\pi/2$ time instances for a plenum pressure of 3.5 bar is shown in Fig. 7. Due to the staggered hole arrangement, the cut plane captures the holes in the first, third, fifth, and seventh rows. At $t-\pi/2$, the cut plane is in the region of expanding gases causing a lower chamber pressure. Due to the lower chamber pressure and an absence of a shockwave, the coolant from all the holes flow freely into the hot gas stream. At time instance of t, the hot and high pressure products are present in the channel at the first two holes which corresponds to first and third row holes in the global hole arrangement. The high pressure gas pushes the hot products into the film cooling holes, but not down the entire length of the hole. At time instance $t+\pi/2$, the oblique shock has passed across the holes and by then the high plenum pressure has pushed the hot gases back out of the holes. However, the high pressure wave from the oblique shock has penetrated inside the coolant plenum as shown in the lowest image in Fig. 7(*b*). Inside the plenum it further dampens out to form acoustic pulsations. These acoustic reflections in the plenum were measured by performing an fast Fourier transform of the pressure signals and found to be twice the detonation frequency. It is unclear at this point if these acoustic waves actually change the amount of hot gas ingestion.

The first two holes highlighted by a dotted rectangle in Fig. 7 corresponds to Rows 1 and 3 in the main staggered hole arrangements. These holes are a region of interest because they are closer to the detonation and experience more hot gas ingestion than the other holes. The hot gas penetration inside the coolant holes for the different plenum pressures is shown in Fig. 8. For a coolant plenum pressure of 3.5 bar, the hot gases only penetrate up to approximately 10% of the hole length at time instance t. Due to the high plenum pressure, the hot gases are quickly flushed back out and hot gases are not visible in the other two time instances. Reducing the plenum pressure to 3 bar causes the hot gases to reach up to 25% of the hole length. The ingestion starts at t with maximum at $t+\pi/2$ and the flow completely recovers by $t-\pi/2$. For the lowest pressure of 2.75 bar, the high product temperatures nearly reach the inlet of the holes. In fact, products, as represented by contours of water vapor in the right side images of Fig. 8, actually do penetrate into the plenum. These hot products dissipate quickly inside the coolant plenum. The water vapor mass fractions are obtained at $t+\pi/2$ to observe the maximum ingestion in each case. Any further reduction in the plenum pressure would result in higher ingestion inside the coolant plenum leading to an increase in coolant temperature. This, therefore, limited the minimum coolant pressure used in this investigation.

The hot gas ingestion due to the oblique shock and the variation of chamber pressure across the circumference changes the mass flux of the coolant in each hole. For a plenum pressure of 3.5 bar, a cut plane through the coolant holes was created as shown in the right hand image of Fig. 9. The black dotted cut plane was taken at 20% along the hole length as shown. The left image shows the contour of mass flux obtained for all the coolant holes at phase

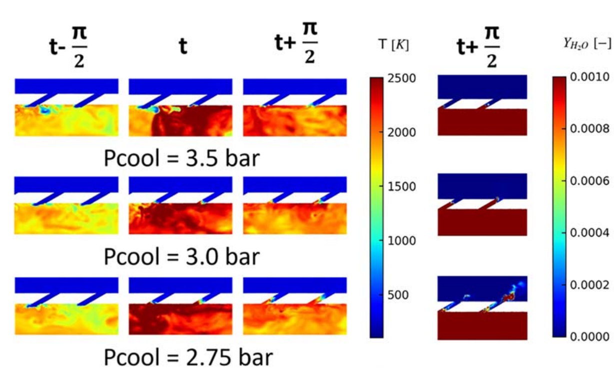

Fig. 8 Temperature contour and water mass fraction of the highlighted region from Fig. 7

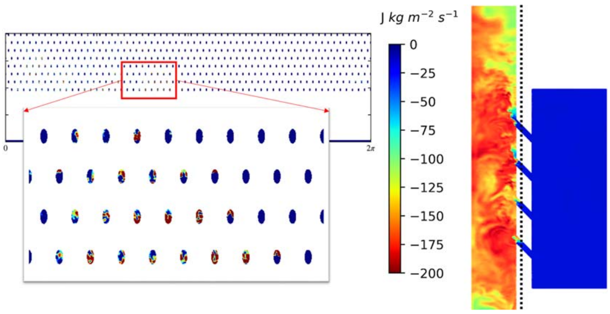

Fig. 9 Contour of hole mass flux for Pcool = 3.5 bar obtained on a cut plane represented by the black dotted line

angle t. A negative mass flux in the contour represents hot gas ingestion into the specific hole. A zoomed in image is subsequently provided to enable better resolution of the cooling holes. In the first row, some holes are completely blocked from the coolant supply due to the presence of high pressure gases. Subsequently, the rows further downstream experience less ingestion due to the reduction in chamber pressure.

Overall, the current cooling scheme involves eight rows of cooling holes. To understand the effect of the oblique shock and the three chamber pressures on the net mass flux in each row, the data obtained from the cut plane across the odd numbered holes are shown in Fig. 10. Each data point in the plot represents a hole and the figure represents the mass flux for each hole at the phase relative to the detonation at π. The circumferential variation in the pressure is principally responsible for the variation of mass flow. The maximum mass flow is observed just ahead of the shock because of the lower local chamber pressure in the combustor. A sudden change in the mass flux is observed when the oblique shock passes across the holes due to the high-pressure spike from the oblique shock. This forces a local flow reversal causing a reduction or even negative mass flux downstream of the shock. For holes further behind the oblique shock, the flow through those holes recovers from the blockage and provides a positive coolant mass flow.

For a plenum pressure of 3.5 bar, the maximum mass flux is observed to be around $300\,\mathrm{kg/m^2\,s}$. Rows 1 and 3 experience more ingestion when compared to the other rows. For Row 1, the oblique shock is at the position π and due to the inclination of the oblique shock, the holes further downstream experience ingestion at a location less than π. Due to the high plenum pressure, the mass flux recovers quickly and by a phase angle of 0 the flow is fully exiting all holes. An overall average coolant mass flow of 112 g/s is achieved. For a plenum pressure of 3.0 bar, the maximum mass flux reduces to around $250\,\mathrm{kg/m^2\,s}$. Due to the reduced plenum pressure with a similar chamber pressure, all the rows experience more ingestion, and the recovery of the mass flux is delayed. The average coolant flow was calculated to be 68 g/s. For a plenum pressure of 2.75 bar, the maximum mass flux reduces to approximately $200\,\mathrm{kg/m^2}s$ and almost all the rows experience more ingestion than the other plenum pressure cases. The recovery is further delayed compared to the 3.0 bar case and the overall mass flow was computed to be 40 g/s.

To attempt to quantify the blockage created by the oblique shock, the holes with negative mass flux in Fig. 10 were considered to be blocked. The number of blocked holes were compared to the total number of holes are plotted as a percentage in Fig. 11 for each row. The blockage increases with a decrease in the coolant plenum pressure due to the lesser potential for recovery with low-plenum pressure. The high-plenum pressure leads to a faster recovery and the blockage in all the holes has reduced significantly. The drawback to the high-coolant plenum is a high coolant mass flow in excess of 25%. In all the cases, the rows closer to the outlet experience less blockage due to a reduced chamber pressure and a weaker oblique shock strength.

An increase in plenum pressure increases the mass flow of coolant, which in turn increases the chamber pressure which

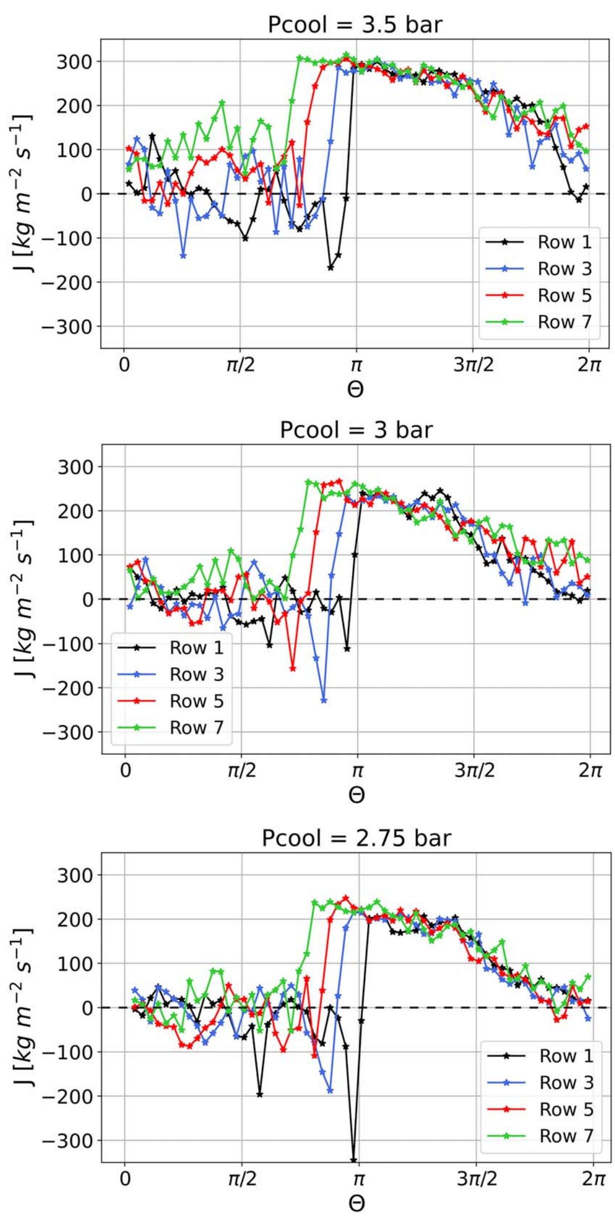

Fig. 10 Mass flux of each hole obtained across the cut plane for the three coolant plenum pressures

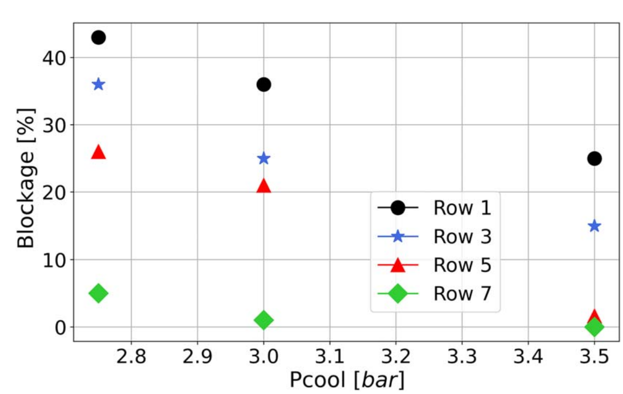

Fig. 11 Percentage of blocked holes in Rows 1, 3, 5, and 7 for the three coolant plenum pressures

subsequently decreases the detonation height as shown in Table 1. The change of detonation height has a secondary impact on the coolant mass flow, specifically in the first three rows, which are closer to the detonation. For a plenum pressure of 2.75 bar, the height of the detonation is 40 cm, and the presence of high pressure products closer to holes induces more backflow and hence the blockage percentage of Row 3 is closer to Row 1. For a plenum pressure of 3 bar, the detonation height reduces to 35 cm reducing the influence of the detonation pressure on the first three rows; hence the difference in blockage between Row 1 and 3 is greater. For a plenum pressure of 3.5 bar, the detonation moves further from the cooling region and the blockage of the first three rows is further reduced.

The temperature in each hole (represented by each data point) was obtained using the cut plane shown in Fig. 9. Figure 12 plots these temperatures for the three plenum pressures where the angular location of each hole is aligned with Fig. 10, namely that with respect to row 1 the oblique shock position is at π. Row 1 in all the cases experience more hot products because it is closer to detonation region. For the rest of the holes, the ingested gas temperature is less due to the decreased pressure downstream from the detonation, enabling less penetration into each subsequent row. Due to high plenum pressure for 3.5 bar, the ingested gases don't reach the cut plane except for Row 1 and hence the temperature in the ingested holes is less when compared to other plenum pressures. For 3.0 bar, Rows 1–3 experience hot gas ingestion and it covers most of the cycle, which means the hot gases stay for a longer time in those holes. However, these gases don't penetrate into the coolant plenum. For 2.75 bar, all the rows experience hot product penetration inside the holes and are observed to be present for almost 75% of the cycle. Furthermore, the hot gases enter the coolant plenum through row 1 confirmed by the water mass fraction contours shown in Fig. 8. The reduction in the chamber pressure effect is more apparent when comparing Row 5. Here, there is little ingestion at the higher pressure, whereas the lower supply pressure of 2.75 bar results in greater temperature inside the holes. The ingestion occurs later in the cycle as well due to the inclination of the oblique shock wave and when it impacts this row.

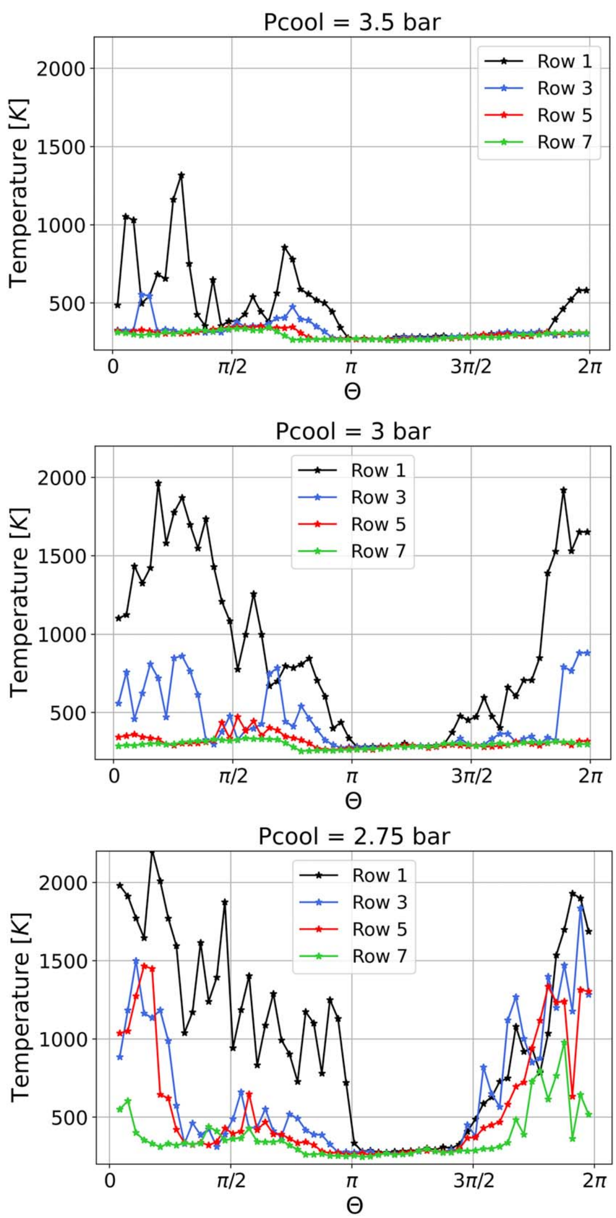

Fig. 12 Temperature in each hole obtained by the cut plane

4.2 Time-Averaged Gas Temperature. The detonation and the oblique shock passes across the holes with an average velocity of 97% CJ velocity. This caused the film layer to be disrupted and rebuilt at this same frequency. To investigate the overall impact of the cooling flow, the quantities are averaged across 30 detonation cycles with a sampling time of 10 μs. The average gas temperature contour obtained for a coolant plenum pressure of 3.5 bar close to the outer wall at 99% of the span is shown in the top left image of Fig. 13. A zoomed in image is shown in the bottom left of the figure. The average temperature profile is similar to a conventional gas turbine film cooling profile. The film builds up with downstream distance resulting in an overall surface temperature reduction from Row 1 to Row 8. The measured minimum gas temperature varies from 1800 K at Row 1 to 1200 K after Row 8. For a plenum pressure of 3.0 bar, the temperature raises to 1850 K at Row 1 and 1300 K after Row 8 due to the reduction in coolant mass flow. Further reducing the plenum pressure to 2.75 bar causes the gas temperature to increase to 1900 K at Row 1 to 1400 K after Row 8. Due to reduced coolant mass flow, and the ingested hot gases over part of the cycle, the film is less protective resulting in the higher temperatures further downstream when compared to other plenum pressures. The film from Rows 1 to 4 in all the cases are disrupted in the contours. However, they still provide cooling and support the further development of the film downstream.

Interestingly, the film flowing out of the first to fourth rows experience a change in the direction because of the tangential velocity component from the detonation wave. The coolant from the subsequent rows flows more axially. This change of film angle (shown in Fig. 13) is similar to gas turbine combustor film holes where the film flow experiences a compound angle due to the tangential component of the swirler flow. As the plenum pressure decreases, the number of rows that have a significant compound angle due to the oblique shock wave increases. For 3.0 bar plenum pressure, Rows 1–5 are influenced by the tangential component of the detonation and oblique shock wave. Additionally, the magnitude of the compound angles are greater than what is experienced by the 3.5 bar case. For the plenum pressure of 2.75 bar, even greater compound angles were experienced for the first three holes while the other holes still are influenced by the swirl from the oblique shock. The compound angle infers that the coolant is not smoothly exiting the hole causing a reduction in its effectiveness. Nevertheless, it still significantly helps in reducing the gas temperature.

4.3 Span-Averaged Gas Temperature. In conventional gas turbine combustors, the film penetration is not significant. The coolant jet might penetrate up to 5% of the combustor channel height. However, in the current film cooling configuration of the TU Berlin RDC, the coolant penetrates up to 50% of the combustor

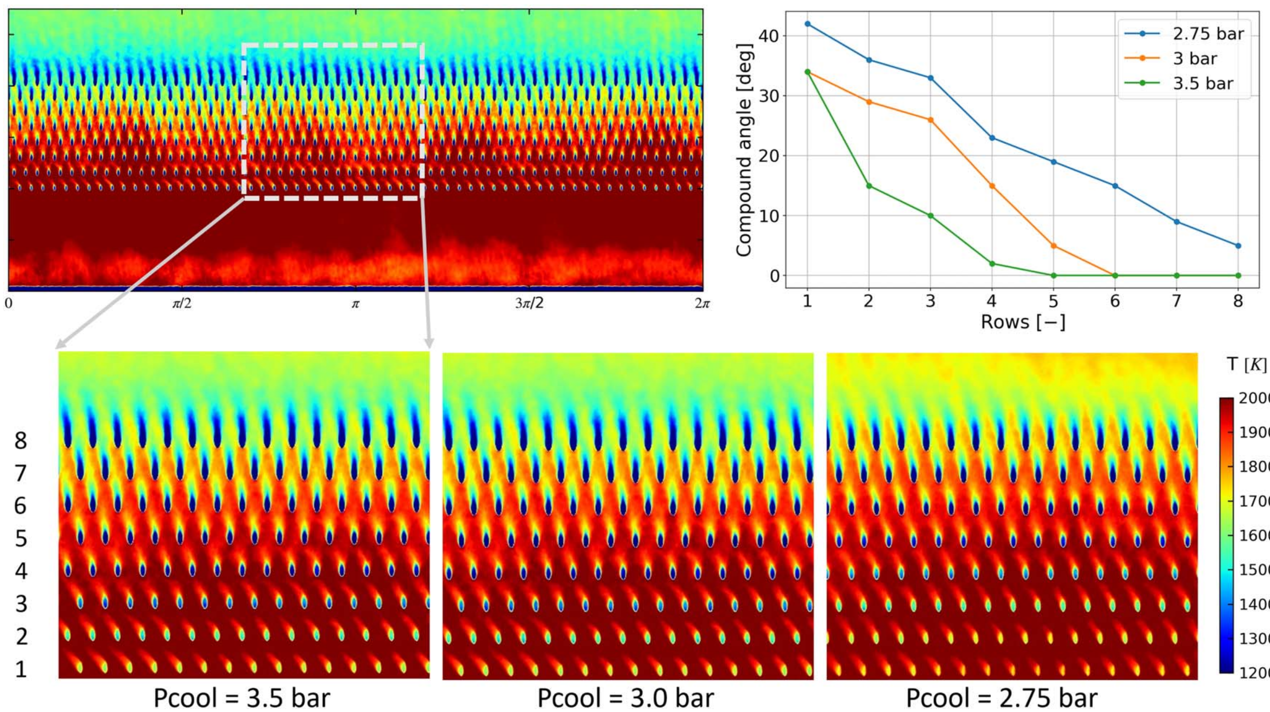

Fig. 13 Contour of gas temperature obtained at 99% of the span along with the measured compound flow angles for the all the plenum pressure cases

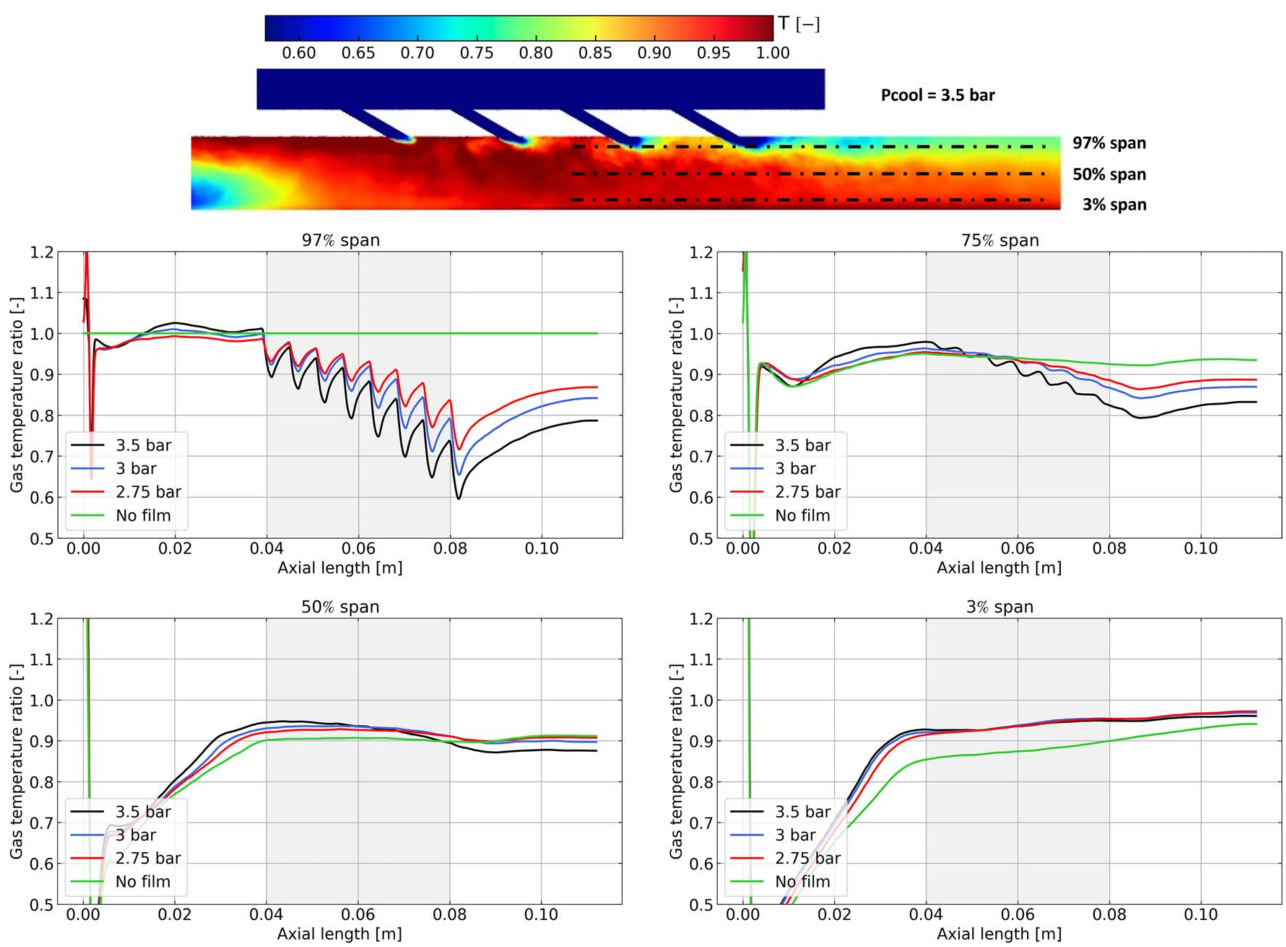

Fig. 14 Temporal and circumferentially averaged normalized gas temperature profiles across 3%, 50%, 75%, and 97% of radial span for all the cases

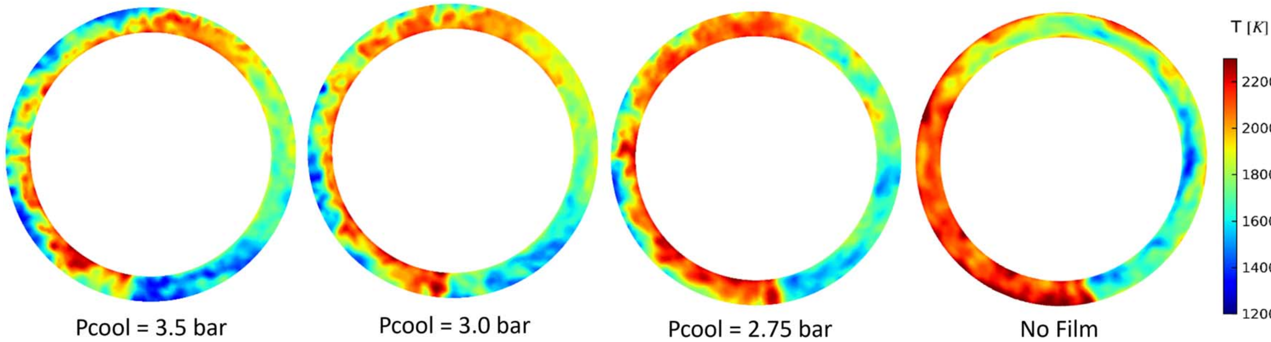

Fig. 15 Outlet temperature contour obtained at the combustor outlet

annulus gap. The penetration of the film can be visualized using the circumferentially averaged and normalized gas temperature profile obtained across different radial spans. The location of the spans is represented by a contour shown in the top image of Fig. 14. The normalization of the gas temperature profiles was referenced to the gas temperature from the uncooled value at 97% and is plotted inFig. 14 where 3% span is closer to the inner wall while 97% is closer to the outer wall where the film cooling holes are located. The shaded region in the plot corresponds to the location of the film cooling holes.

At 97% span, the temperature profiles for the film cooled cases show a reduction from the uncooled baseline. The highest temperature reduction occurs for a plenum pressure of 3.5 bar. The reduction in temperature starts with the axial location of 4 cm where the first row of film holes is located. The temperature tends to decrease till 8 cm where the last row of holes is situated. Then the gas temperature increases as it progresses toward the outlet.

As the plenum pressure is reduced to 3.0 bar, the mass flow of coolant is reduced to 68 g/s. The reduction in mass flow resulted in higher gas temperatures for 3.0 bar than the 3.5 bar case. Higher gas temperatures were obtained for a plenum pressure of 2.75 bar where the reported mass flow is 40 g/s. However, in the film cooling region, a 40% gas temperature reduction was observed compared to the uncooled case. Although the plenum pressure of 2.75 bar experiences hot product ingestion inside the coolant plenum, it still performs sufficiently well in terms of reducing the gas temperature.

The gas temperature in the 75% span behaves similarly to the 97% span. The gas temperature is lower for 3.5 bar and it increases as the plenum pressure is decreased. The penetration of the coolant is much stronger for 3.5 bar as the wiggles in the film cooled region are much stronger than the other cases. Interestingly, the gas temperature of film cooled cases below an axial length of 0.04 m is greater than the uncooled case. This is because of the effect of film cooling fluid pushing the hot products toward the inner wall. This is more visible in the plot of 50% span. The gas temperature at 50% span for the film cooled cases is always greater than the uncooled case until an axial length of 0.08 m. After 0.08 m, the temperatures are reduced because the mixing of the cold film gases with the hot products. However, for 3% span it is clearly visible that the gas temperature for the cooled cases is always greater than the uncooled case across the entire axial length. This shows that due to small annulus width and high jet penetration to the main stream, the hot products are pushed toward the inner wall. The temperature contours obtained at the outlet of the combustor depicted in Fig. 15 clearly show the increase in hot product distribution at the inner wall. This leads to an increase in heat transfer in the inner wall. A likely outcome of this result is the requirement to also provide film cooling on the inner wall.

The gas temperature closer to the outer wall corresponding to 97% of the span shows a benefit in using film cooling for RDC. The gas temperature is significantly reduced, however, the wall temperature is expected to be lower than the gas temperature. A plenum pressure of 2.75 bar, even with gas hot ingestion to the coolant plenum, performs sufficiently well in terms of cooling. Hence, film cooling can be a possible solution for RDC cooling.

5 Conclusion

RDCs, due to a small annulus width and the detonation process, experience heat loads that are significantly higher when compared to conventional gas turbine combustors. Film cooling could be one of the possible cooling strategies for the RDC. However, to date, there have been no experimental studies of film cooling within an RDC. Numerically, only a couple of single row investigations have been performed. Leaving the question as to whether film cooling can even be applied within an RDC unanswered. To investigate the possibility of film cooling for RDC, the TU Berlin RDC architecture was modified by adding film cooling holes and a coolant plenum. Large eddy simulation of the film cooled RDC was performed using the AVBP solver utilizing a single-step reaction mechanism.

Three plenum pressures of 2.75, 3.0, and 3.5 bar were selected corresponding to 9%, 16%, and 26% of the overall combustor mass flow to replicate the range of realistic GT combustor liner cooling flows. Coolant mass injection into chamber naturally maintained a pressure ratio of around 1.75 by creating a fluidic blockage and back pressurizing the detonation. This phenomena is likely beneficial in that the film cooling flow helps to back pressurize the detonation and therefore it helps strength the detonation wave. For all three pressures, the oblique shock downstream of the detonation created variation in the coolant mass flow out of each hole with each wave passing. Specifically, for a portion of the cycle the flow out of the coolant hole was blocked and local flow reversal occurred in the cooling holes. This blockage was found to be more for 2.75 bar and was reduced as the plenum pressure was increased. The portion of the cycle that was blocked reduced with downstream location for all the plenum pressures because of the lower local chamber pressure and a weaker oblique shock at that location.

The presence of oxygen in the coolant flow generated additional deflagrative heat release. This heat release was cyclic with the passing of the oblique shock. As the cooling film builds up, this secondary burning is stood off from the wall. As such, film cooling could aid in the overall combustion efficiency by consuming residual fuel. Furthermore, the film flowing out of holes experienced a compound angle due to the tangential component of velocity induced by the rotating detonation and oblique shock wave. This angle was as much as 40 deg for Row 1 reducing in angle with both downstream distance and plenum pressure but does suggest the possibility of aligning the film holes tangentially to reduce the ingestion.

Overall, the penetration of the cooling jets was high, but even with this configuration, the gas temperature at the outer wall was significantly reduced by the film cooling. A film was able to form along the outer diameter of the RDC and the average gas temperature for the 3.5 bar case was reduced from 2100 K to 1300 K at the end of the film cooled region. As the coolant mass flow was decreased, the gas temperature increased as expected. Interesting was that coolant ejection along the outer wall had an impact on the gas temperatures across the span of the RDC. The presence of the film pushed the hot gases radially inward (toward the inner wall). Overall, the gas temperature and ingestion response show that film cooling is possible for an RDC and the unsteadiness generated by the oblique shock can be overcome.

Acknowledgment

This project has received funding from the European Union's Horizon 2020 Research and Innovation Program under the Marie Skłska-Curie Grant Agreement No. 956803. The authors also thank Pier Carlo Nassini for his support.

Conflict of Interest

There are no conflicts of interest.

Data Availability Statement

The datasets generated and supporting the findings of this article are obtainable from the corresponding author upon reasonable request.

Nomenclature

J = mass flux (kg/m^2 s)
$\dot{m}$ = mass flow (kg/s)
Pcool = coolant plenum pressure (bar)
Pchamber = chamber pressure (bar)
Θ = angle (deg)
μ = viscosity ($N - s/m^2$)
Φ = hole diameter (mm)

Superscripts and Subscripts

air = air flow
coolant = coolant flow
fuel = fuel flow
sg = sub grid
v = viscosity

Acronyms

GT = gas turbine
NSCBC = Navier–Stokes characteristic boundary conditions
PGC = pressure gain combustor
RDC = rotating detonation combustor

References

[1] Anand, V., and Gutmark, E., 2019, "Rotating Detonation Combustors and Their Similarities to Rocket Instabilities," Prog. Energy. Combust. Sci., **73**(2), pp. 182–234.
[2] Lee, J. H., Ryu, J. H., Lee, E. S., Han, H. S., and Choi, J. Y., 2023, "Experimental Proof of Concept of a Noncircular Rotating Detonation Engine (RDE) for Propulsion Applications," Aerospace, **10**(1), p. 27.
[3] Dechert, J. R., Schauer, F., Polanka, M. D., Schumaker, S. A., Sell, B. C., and Fotia, M. L., 2020, "Development of a Small Scale Rotating Detonation Engine," AIAA SciTech Forum, Vol. **1 PartF**, pp. 1–11.
[4] Wyatt, J. J., Snow, N. J., Fiorino, N. T., Schauer, F. R., Polanka, M. D., Sell, B. C., and Cho, K. Y., 2022, "Injection Studies on a Small-Scale Rotating Detonation Engine," AIAA SciTech Forum 2022, pp. 1–11.
[5] Fiorino, N. T., Snow, N. J., Schauer, F. R., Polanka, M. D., Schumaker, S. A., and Sell, B. C., 2023, "Improving Detonability in a Small-Scale Rotating Detonation Engine Using Partial Premixing," J. Propul. Power, **39**(2), pp. 232–241.
[6] Nassini, P. C., 2022, "High-Fidelity Numerical Investigations of a Hydrogen Rotating Detonation Combustor," Ph.D. Thesis, UniFI, Firenze.
[7] Theuerkauf, S. W., King, P. I., Schauer, F. R., and Hoke, J. L., 2013, "Thermal Management for a Modular Rotating Detonation Engine," AIAA Aerospace Sciences Meeting, pp. 1–9.
[8] Theuerkauf, S. W., Schauer, F. R., Anthony, R., and Hoke, J. L., 2014, "Average and Instantaneous Heat Release to the Walls of an RDE," AIAA SciTech.
[9] Theuerkauf, S. W., Schauer, F. R., and Anthony, R., 2015, "Experimental Characterization of High-Frequency Heat Flux in a Rotating Detonation Engine," AIAA SciTech., pp. 1–10.
[10] Theuerkauf, S. W., Schauer, F. R., and Anthony, R., 2016, "Comparison of Simulated and Measured Instantaneous Heat Flux in a Rotating Detonation Engine," AIAA SciTech.
[11] Meyer, S. J., Polanka, M. D., Schauer, F. R., Anthony, R. J., Stevens, C., Hoke, J. L., and Rein, K., 2017, "Experimental Characterization of Heat Transfer Coefficients in a Rotating Detonation Engine," AIAA Aerospace Sciences Meeting, January, pp. 1–11.
[12] Meyer, S. J., Polanka, M. D., Schauer, F. R., and Hoke, J. L., 2018, "Parameter Impact on Heat Flux in a Rotating Detonation Engine," AIAA Aerospace Sciences Meeting, January, pp. 1–10.
[13] Goto, K., Nishimura, J., Kawasaki, A., Matsuoka, K., and Kasahara, J., 2018, "Propulsive Performance and Heating Environment of Rotating Detonation Engine With Various Nozzles," J. Propul. Power, **35**(1), pp. 1–11.
[14] Sandri, U., Ramanagar S, S., Andreini, A., and Myles, B. D., 2024, "Evaluation of Cooling Requirements for Rotating Detonation Combustors," ASME J. Turbomach., **146**(5), p. 051004.
[15] Tian, J., Wang, Y.-S., Zhang, J.-Z., and Tan, X.-M., 2022, "Numerical Investigation on Flow and Film Cooling Characteristics of Coolant Injection in Rotating Detonation Combustor," Aerospace Sci. Technol., **122**(1), p. 107379.
[16] Yu, J., Yao, S., Li, J., Huang, Y., Guo, C., and Zhang, W., 2022, "Effects of Inlet and Secondary Flow Conditions on the Flow Field of Rotating Detonation Engines With Film Cooling," Int. J. Hydrogen Energy, **48**(24), pp. 9082–9094.
[17] Li, R., Xu, J., Lv, H., Lv, D., and Song, J., 2023, "Numerical Investigations of the Nozzle Performance for a Rocket-Based Rotating Detonation Engine With Film Cooling," Aerospace Sci. Technol., **136**(1), p. 108221.
[18] Bach, E., Stathopoulos, P., Paschereit, C. O., and Bohon, M. D., 2020, "Performance Analysis of a Rotating Detonation Combustor Based on Stagnation Pressure Measurements," Combust. Flame., **217**(4), pp. 21–36.
[19] Bach, E., Bohon, M. D., Paschereit, C. O., Berlin, T. U., and Dynamics, F., 2018, "Development of an Instrumented Guide Vane Set for RDC Exhaust Flow Characterization".
[20] Nassini, P. C., Andreini, A., and Bohon, M. D., 2023, "Characterization of Refill Region and Mixing State Immediately Ahead of a Hydrogen-Air Rotating Detonation using LES."
[21] Schonfeld, T., and Rudgyard, M., 1999, "Steady and Unsteady Flow Simulations Using the Hybrid Flow Solver AVBP," AIAA J., **37**(11), pp. 1378–1385.
[22] Gicquel, L. Y., Gourdain, N., Boussuge, J. -F., Deniau, H., Staffelbach, G., Wolf, P., and Poinsot, T., 2011, "High Performance Parallel Computing of Flows in Complex Geometries," Compt. Rendus. Mécanique, **339**(2–3), pp. 104–124.
[23] Gicquel, L., Staffelbach, G., and Poinsot, T., 2012, "Large Eddy Simulations of Gaseous Flames in Gas Turbine Combustion Chambers," Prog. Energy Combust. Sci., **38**(6), pp. 782–817.
[24] Barré, D., Kraushaar, M., Staffelbach, G., Moureau, V., and Gicquel, L. Y., 2013, "Compressible and Low Mach Number LES of a Swirl Experimental Burner," Compt. Rendus. Mécanique, **341**(1–2), pp. 277–287.
[25] Ramanagar, S., Andreini, A., Polanka, M. D., and Bohon, M. D., 2024, "The Impact of Film Cooling on the Heat Release Within a Rotating Detonation Combustor," Appl. Energy Combust. Sci., **20**(1), p. 100300.
[26] Dupuy, D., Perrot, A., Odier, N., Gicquel, L., and Duchaine, F., 2021, "Boundary-Condition Models of Film-Cooling Holes for Large-Eddy Simulation of Turbine Vanes," Int. J. Heat Mass Transfer, **166**(1), p. 120763.
[27] Aillaud, P., Duchaine, F., Gicquel, L. Y. M., Koupper, C., and Staffelbach, G., 2017, "Large Eddy Simulation of Trailing Edge Cutback Film Cooling: Impact of Internal Stiffening Ribs on the Adiabatic Effectiveness," 7th European Conference for Aeronautics and Aerospace Sciences (EUCASS) (1), pp. 1–14.
[28] Shum-Kivan, F., Duchaine, F., and Gicquel, L., 2014, "Large-Eddy Simulation and Conjugate Heat Transfer in a Round Impinging Jet," In Volume 5A: Heat Transfer, Vol. 5A, American Society of Mechanical Engineers, pp. 1–11.
[29] Agarwal, S., Gicquel, L., Duchaine, F., Odier, N., and Dombart, J., 2021, "Analysis of the Unsteady Flow Field Inside a Fan-Shaped Cooling Hole Predicted by Large Eddy Simulation," ASME J. Turbomach., **143**(3), p. 031011.
[30] Celik, I. B., Cehreli, Z. N., and Yavuz, I., 2005, "Index of Resolution Quality for Large Eddy Simulations," ASME J. Fluids Eng., **127**(5), pp. 949–958.
[31] Lefebvre, A. H., and Ballal, D. R., 2010, *Gas Turbine Combustion Alternative Fuels and Emissions*, Vol. 132, CRC Press, Boca Raton, FL.
[32] Carusotto, S., Goel, P., Baratta, M., Misul, D. A., Salvadori, S., Cardile, F., Forno, L., Toppino, M., and Valsania, M., 2022, "Combustion Characterization in a Diffusive Gas Turbine Burner for Hydrogen-Compliant Applications".
[33] Polanka, M. D., Zelina, J., Anderson, W. S., Sekar, B., Evans, D. S., Lin, C. X., and Stouffer, S. D., 2011, "Heat Release in Turbine Cooling I: Experimental and Computational Comparison of Three Geometries," J. Propul. Power, **27**(2), pp. 257–268.
[34] Anderson, W. S., Polanka, M. D., Zelina, J., Evans, D. S., Stouffer, S. D., and Justinger, G. R., 2010, "Effects of a Reacting Cross-Stream on Turbine Film Cooling," ASME J. Eng. Gas Turbines Power, **132**(5), p. 051501.